Appl Magn Reson
DOI 10.1007/s00723-012-0435-5

Applied
Magnetic Resonance

# Pulsed Electron Spin Resonance Ex Situ Probe for Tooth Biodosimetry

**Ksenia Sirota · Ygal Twig · Aharon Blank**

Received: 13 September 2012 / Revised: 14 November 2012


**Abstract** An electron spin resonance (ESR) probe that includes a static field source and a microwave resonator for the measurement of paramagnetic defects in tooth enamel is presented. Such defects are known to be a good marker for quantifying the amount of ionizing radiation dose absorbed in the tooth. The probe can measure the tooth when it is positioned just above its outer surface, i.e., in ex situ geometry. It is operated in pulsed mode at a frequency of $\sim$6.2 GHz that corresponds to the magnitude of the static magnetic field of its permanent magnet. A detailed design of the probe is provided, together with its specifications in terms of measurement volume and signal-to-noise-ratio for a typical sample. Experimental results that verify its sensitivity and capability to measure gamma-irradiated teeth are provided. The current minimal detected signal by the probe corresponds to a radiation dose of $\sim$4 Gy.

## 1 Introduction

Electron spin resonance (ESR) is a very useful and robust spectroscopic method with many applications in science and technology [1]. However, its clinical use is limited (compared to its "brother"—nuclear magnetic resonance imaging), partly because of the need to introduce exogenous paramagnetic species into the subject to facilitate ESR measurements. One exception is the measurement of stable radicals induced by ionizing radiation in bones and teeth [2, 3]. They make it possible to quantify the radiation absorbed dose in the irradiated organ. Such type of quantification can be related to the more broadly classified array of biodosimetry methods, which are defined as methods for retrospectively measuring the amount of ionizing radiation dose received by an individual using only biological materials.

K. Sirota · Y. Twig · A. Blank (✉)
Schulich Faculty of Chemistry, Technion, Israel Institute of Technology,
32000 Haifa, Israel
e-mail: ab359@tx.technion.ac.il

Published online: 24 January 2013

The use of ESR signals in tooth enamel as a dosimetric detector has been known for more than four decades. Most of the work was carried out on extracted teeth, but recently several in vivo systems have also been developed [2]. The tooth enamel is very useful for this purpose, since, as has been suggested in the past, stable $CO_2^-$ radicals are generated in the carbonate impurities of its calcium-based mineral hydroxyapatite [4].

Humans can be exposed to ionized radiation in a variety of circumstances, such as X-ray scans, prolonged flight periods, and due to other environmental factors. In such "normal" cases, biodosimetry can be carried out using accurate *biological* methods such as dicentric chromosome assay, which involves examining chromosomes for characteristic damage caused by ionizing radiation. However, this process is relatively complicated and takes more than 2 days from the time of exposure to reach a conclusion [5]. Moreover, some scenarios require a much faster *physically* based diagnostic method, such as ESR-based biodosimetry. Examples of these scenarios are major nuclear events, such as a nuclear power plant accident or the detonation of a nuclear device (either a bomb or a radiological dispersal device—also known as a "dirty bomb"). In such cases, there is a need to determine the magnitude of the exposure by measuring the radiation dose absorbed by the persons involved. In many of the scenarios, this determination has to be carried out very soon after the event for thousands of individuals and while the subjects are still present at the health-care site.

In view of these needs, significant progress has been recently made regarding the use of ESR-based biodosimetry techniques for the detection of radiation absorbed dose in human teeth and their incorporation into a transportable in vivo system [6]. Initial designs involved relatively large electromagnets, while more recent versions make use of smaller magnets and spectrometers, with an emphasis on improved sensitivity and field deployment [7, 8].

Despite this progress, current operating systems and published future designs aimed at in vivo biodosimetry based on the ESR signal of a tooth still suffer from the following limitations:

1. *Use of relatively large and heavy magnets*: Most ESR systems for teeth biodosimetry are based on the use of large electromagnets. These are suitable for work in a laboratory setup; however, such an approach is clearly not desirable for field-deployable systems and even in fixed locations at hospitals, due to weight, power requirements, and relatively high costs.
2. *Resonator/tooth/magnet alignment problems*: Some recent designs offer the possibility of using smaller magnets, either electrically powered or permanent ones [6]. These can potentially improve upon the use of laboratory electromagnets. However, small magnets have a relatively low homogenous volume that is very close to the size of a tooth, $\sim$0.5–1 ml. This creates a major limitation related to the difficulty in aligning the resonator and tooth with the sensitive volume of the magnet's center.
3. *Whole-tooth measurements*: In vivo systems traditionally make use of relatively low-frequency ($\sim$1–2 GHz) ESR spectroscopy due to microwave (MW) field penetration issues. At these frequencies, sensitivity is rather low and the

measurement of a whole tooth (and sometimes two of them) is required to obtain a sufficiently clear signal. The measurement of a complete tooth may lead to reduced accuracy due to unknown tooth volume and the effects of cavities and surface defects. Uncertainty regarding tooth volume is a major concern, because it is known that the concentration of paramagnetic defects in the enamel is proportional to the radiation dose (around $2.8 \times 10^{13}$ spins $Gy^{-1}$ $g^{-1}$ [9]); however, to provide the spin *concentration* from the measured ESR signal, the measured tooth *volume* must be accurately determined (which, as noted above, is a problem for an arbitrary selected tooth). Furthermore, when measuring a whole tooth, consideration should be given to the separate signal originating in the dentin (which has a different response to ionizing radiation) as opposed to the enamel-based signal, and also to the quantification of the ratio between the two.

4. *Limitations in measuring teeth in children, toddlers, and babies*: Younger children's teeth are usually too small to obtain a good ESR signal in L-band in vivo systems. Furthermore, many toddlers and babies lack molar teeth. Since on average more than 20 % of the population in the USA is younger than 14 years of age [10] (and in some countries, this is more than 40 %), it is important to provide a solution also for this sector.
5. *Disposable items and measurement costs*: The use of resonators and/or magnets that are placed inside the mouth raises the need for disposable/sterile components that complicate the system and increase measurement costs.
6. *The limitation of continuous wave (CW) operation*: Most in vivo ESR systems operate in CW mode, which brings with it quite a long list of difficulties. To get a good signal in CW ESR, the use of resonators that are well matched and tuned with a relatively high quality factor ($Q$) is required. The matching and tuning process can be quite cumbersome and must be automated for the non-expert user. Moreover, movement by the subjects further complicates this issue and increases measurement baseline distortions and "noise".
7. *Limited spin sensitivity*: Even under optimal operating conditions, the use of relatively low-frequency CW ESR results in quite limited spin sensitivity. This leads to an inaccurate estimation of the radiation dose, which is currently found to be $\sim$1.5–2 Gy for a few minutes of measurement time [7]. This value is higher than the minimum acceptable level of error for proper patient diagnostics, which is at least 0.5 Gy and preferably 0.25 Gy. Such error level is considered as a minimum requirement needed for proper triage following a major nuclear event. The common practice in such cases is that one needs to be able to differentiate between persons exposed to less than 2 Gy who do not need any treatment, persons exposed to 2–6 Gy who would need immediate treatment and can recover, and persons exposed to more than 6–8 Gy who cannot be saved [11].

In view of the above, it is evident that while the basic physical feasibility of in vitro and in vivo tooth dosimetry by ESR is well established, there is still plenty of room for improvement in aspects related to the practical implementation of this method. Many characteristics of the issue at hand hint at the possibility that

conventional in vivo CW ESR methodologies may not be the best way to tackle the problem. For several years now, it has been known in the field of nuclear magnetic resonance (NMR) that, for purposes of examining a specific small region within a large sample, it could be highly advantageous to obtain NMR information by using a small self-contained probe (with a magnet and radiofrequency coils) that can be attached to the surface of the sample or inserted into it, thus avoiding the requirement for a large external magnet. Such an approach to NMR measurement or NMR imaging without a sample-surrounding magnet is termed "inside-out" or ex situ NMR [12–17]. Several types of NMR systems operating in an inside-out geometry are already in existence and show capabilities of measuring relaxation parameters [18, 19], diffusion coefficients [20], and 3D imaging [21]. Most of these ex situ NMR probes are intended for materials science applications; however, recent developments (some of them from our group) have shown the validity of such compact probes also for specific medical applications [22–26]. Up until now, ex situ methodology was applied only to NMR and no probes were developed for ESR applications. As for the CW operation, in view of the above-mentioned limitations, it would be highly advantageous to pursue a pulsed acquisition method. Traditionally, due to the broad (inhomogeneous) linewidth of the tooth signal, it was thought that $T_2$ was too short for pulsed measurements. However, a recent study has shown that the relaxation times in irradiated teeth are sufficiently long to facilitate such acquisition mode, even at room temperature [27]. Nevertheless, until now, no system or probes have been developed for pulsed ESR biodosimetry of teeth.

In this work, we make use of our previously developed ex situ NMR methodologies and combine them with our miniature ESR resonators [28] to come up with the first compact pulsed ex situ ESR probe for biodosimetry based on measurements of incisor teeth. We will provide a detailed description of our probe along with some representative experimental results, followed by discussion of its sensitivity and applicability as a deployable in vivo ESR biodosimetry system, and the future prospects of our approach.

## 2 Technical Description of the Probe

A general drawing of the ex situ ESR biodosimetry probe is provided in Fig. 1, along with an artist's concept of its presumed operation technique. The probe operates with our home-made pulsed ESR system [28] and provides echo ESR signals from the incisor tooth attached to it that are directly proportional to the amount of radiation absorbed dose. We will now describe the reasoning leading to this design.

### 2.1 Design Approach

Our goal is to measure ESR signals from the teeth while these are inside the patient's mouth. It is well known that the amplitude of the ESR signals is proportional to the spin concentration multiplied by the tooth volume. The spin concentration is the number we seek, since it is in linear correlation with the

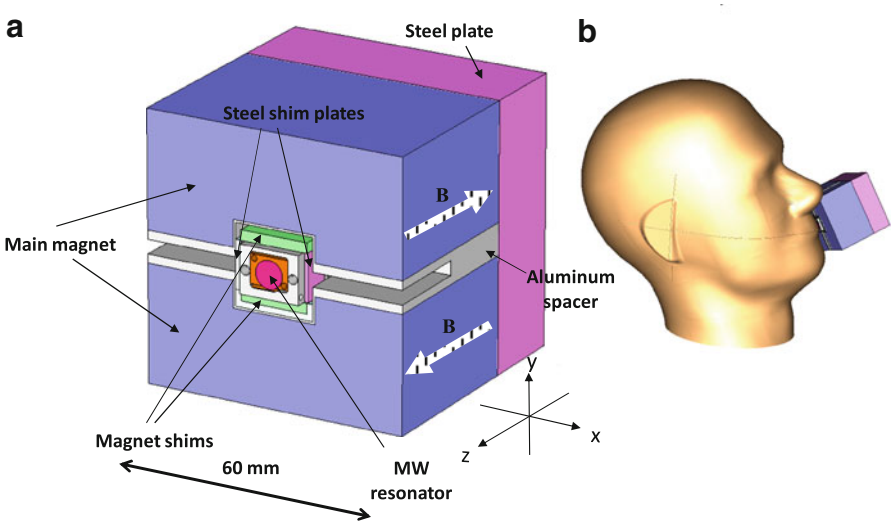


**Fig. 1** **a** Drawing of the ex situ ESR probe structure, showing the main magnet, its shim units, and the microwave resonator. **b** An "artist's concept" of the probe during operation (color figure online)

radiation dose. The main limiting factor of ESR-based biodosimetry is achieving enough signal-to-noise-ratio (SNR) at a given measurement time. It is known that for a given static magnetic field, the signal increases with the volume of the measured sample (assuming a fixed spin concentration). SNR also improves significantly when operating at higher static fields. When measuring soft tissues, the depth of penetration does not allow the use of static fields that are higher than $\sim$0.03–0.04 T (i.e., a frequency of $\sim$1.5 GHz). Still, the teeth are not soft tissue and thus, if the resonator's operation is restricted to the tooth's immediate region, it can be used also at much higher fields. Our design therefore features the use of a much higher static field than is normally employed in in vivo ESR (currently $\sim$0.22 T). This enables us to considerably reduce the measurement volume from a typical $\sim$0.5–1 mL for a whole tooth (only $\sim$1/10 of which is actual enamel) down to $\sim$1 μL of pure tooth enamel (i.e., a reduction by $\sim$3 orders of magnitude), while still maintaining the same level of SNR. In addition, the use of pulsed ESR rather than CW ESR makes the system much less susceptible to static field inhomogeneities (since these can be refocused by standard echo techniques). Thus, the combination of elevated fields, a small volume of interest, and a pulsed mode of operation facilitates the use of a much smaller magnet that does not have to enclose the measured volume, but rather can be situated near it, in ex situ geometry.

## 2.2 The Magnet

The magnet's design is shown in Figs. 1 and 2. It is composed of two large blocks and two small shim units made of temperature-compensated samarium-cobalt (SmCo) permanent magnets (material #EEC2:17TC-16 from Electron Energy Corporation, USA) with a remanence of 0.83 T and a temperature coefficient of

−10 ppm/C. The two large U-shaped magnet parts have opposite magnetization direction (one along the positive and one along the negative $Z$ axis; see Fig. 1) and are placed on a 1010-steel yoke with a gap between them, as shown in Fig. 2. Thus, the magnetic field direction in the region of interest (just above the magnet's surface at the center) is along the $Y$ axis. Two small shim units are placed in the gap (shown in green in Fig. 1) and have [$X$, $Y$, $Z$] dimensions of [15.6, 2.3, 6] mm, respectively, in agreement with the coordinates in Fig. 1. (The origin of our coordinate system is the center point on the upper surface of the main magnets.) Each shim unit has an opposite direction of magnetization with respect to its neighboring large magnet piece. In addition, there are two small 1010-steel blocks that improve the field's shimming (placed in the gap, as shown in Fig. 1) that are [1, 6, 10] mm in size. The entire magnet is capped on the sides by 6.3-mm-thick aluminum plates and on the top by 0.5-mm-thick plates to prevent accidental damage.

The philosophy behind this design is to generate a sweet spot with modest field homogeneity just above the magnet's upper surface and a gradient of $\sim$1 T/m just below this spot (closer to the magnet's surface). This spot, or its adjacent 1 T/m gradient area, are both good candidates for "the volume of interest" from which the ESR signal is to be acquired. The sweet spot was used in our current experiments to maximize the measured volume, while the "gradient area" may be used (in the future) for 1D imaging along the $Z$ axis. The geometry of the shim plates was optimized in our calculations, so that, in combination with the main unit, the total magnetic field to be generated has the desired spatial dependence. Figures 3 and 4 present the static field magnitude in various positions in and around the volume of interest, calculated using Maxwell finite element software (Ansoft Corporation, Pittsburgh, PA, USA) and measured by a 100-μm Hall probe sensor (model 3RT100-2-2, Sentron, Zug, Switzerland). The sweet spot and the gradient area are clearly visible above the magnet's surface. The exact position and nature of the sweet spot and the gradient depend on the shim units' properties and position. We placed the center of the magnet shim units at locations [0, ±7.7, −3] mm with

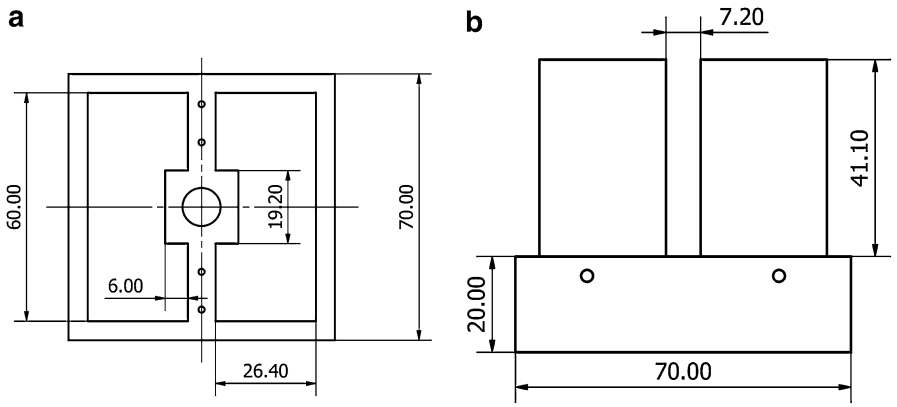


**Fig. 2** Drawing of the main magnet's parts and their steel back plate. **a** View from above. **b** View from the side

respect to the global magnet coordinates. The measured results were found to be satisfactory in the first assembly iteration (but if needed, it is possible to re-iterate on the shim units' location and improve the fit between theory and experiment). The 2D surface plots of the static field in the *XY* plane (Fig. 4) also show a satisfactory resemblance between the measured and calculated data, especially regarding homogeneity around the peak position. Figure 5 provides pictures of the assembled probe and the computer-controlled static field mapping apparatus. The plastic pieces that protrude from the magnet's surface hold the small shim magnets and allow us to move them in or out of the probe, if needed (but they, of course, will not be included in an actual working in vivo assembly).

### 2.3 The Resonator

The microwave resonator is presented in Fig. 6. It is a dielectric ring resonator manufactured using a titanium dioxide ($TiO_2$—rutile) single crystal. This crystal has high anisotropic permittivity with values of 165 and 85 (unitless, compared to the free-space permittivity) along the resonator's *X* and *Y* axes, respectively (at room temperature). The resonator's dimensions are: outer diameter 6.3 mm, inner diameter 0.8 mm, and height 1.5 mm. They were determined via finite element calculations (CST Microwave Studio, CST GmbH, Germany) to sustain a resonance frequency of 6.185 GHz for the fundamental $TE_{01\delta}$ mode (see Fig. 6a) that matches the static field of the permanent magnet. The resonator is excited by a loop at the end of a thin (1.5 mm o.d.) semi-rigid coaxial transmission line (Fig. 6b). In order to fine-tune the resonance frequency, we placed a small coaxial screwable stub coated with Rexolite close to the resonator (Fig. 6c). The spot where the magnetic field is optimal (marked with a green circle in Fig. 6a) is aligned automatically with the resonator's location because the magnet and the resonator's structure are mechanically fixed together and brought forward toward the tooth. The resonator's quality factor was measured using a vector network analyzer (E8361A, Agilent Technologies, USA) and was found to be $Q_L \sim 250$ (i.e., unloaded $Q_u \sim 500$). The effective resonator volume [29, 30] was calculated from the finite element simulation results and was found to be $V_c \sim 35$ μL.

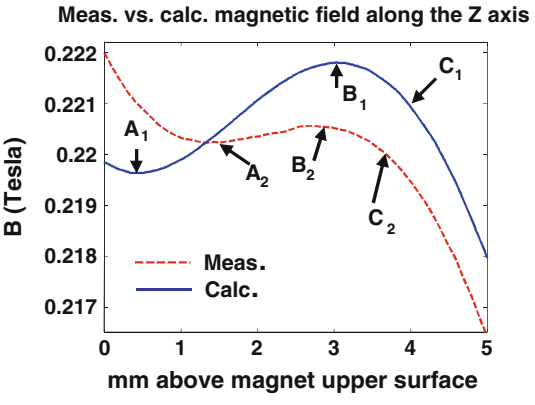


**Fig. 3** Calculated and measured static magnetic field magnitude as a function of the position along the *Z* axis (*X*, $Y = 0$), where $Z = 0$ is the magnet's upper surface

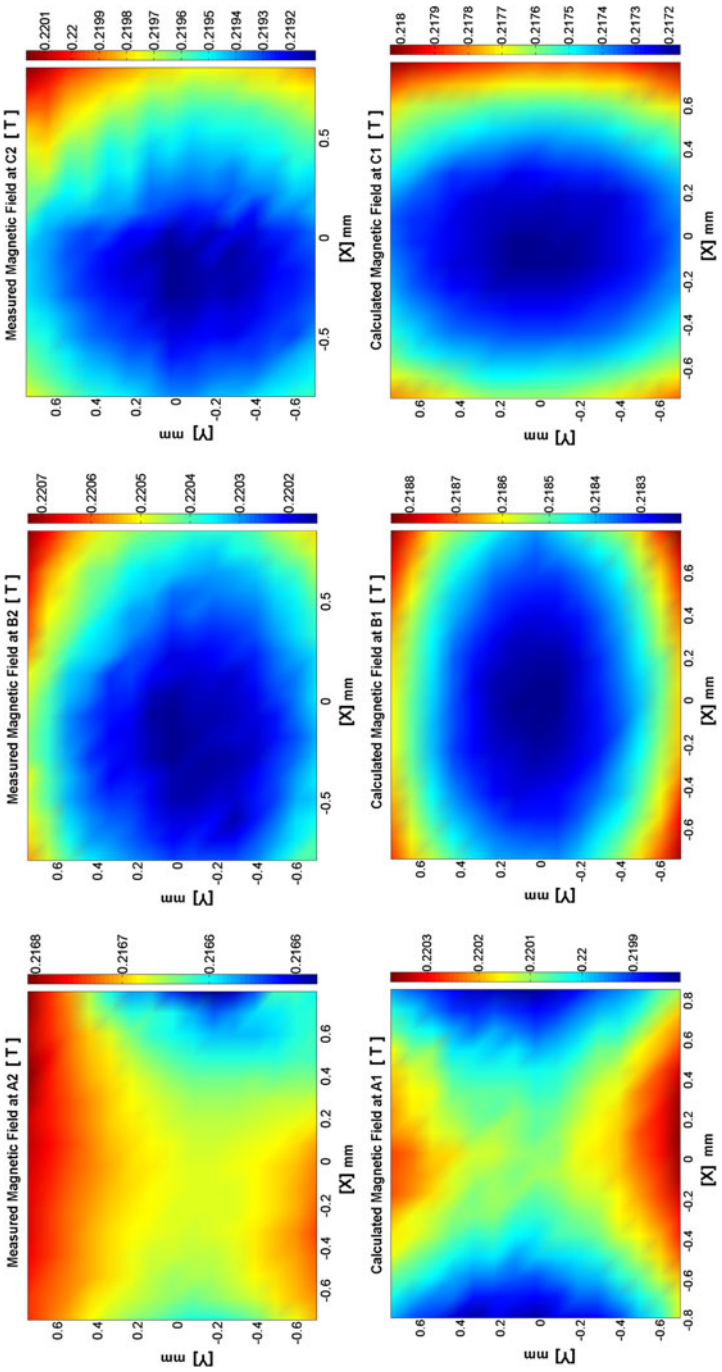


**Fig. 4** Calculated (*lower plates*) and measured (*upper plates*) static field magnitude at several *XY* planes situated in different *Z* locations, as marked in Fig. 3

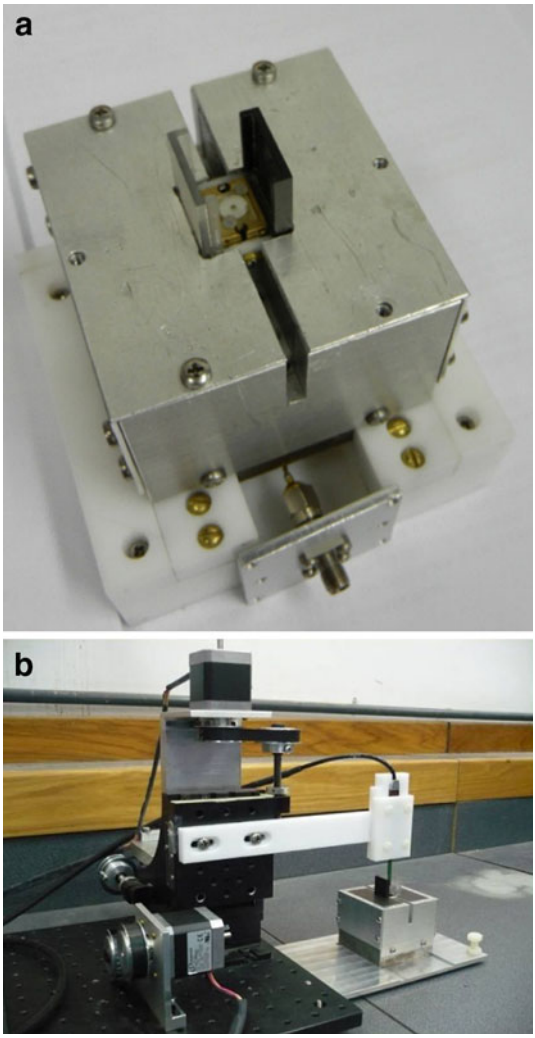


**Fig. 5** **a** Photo of the assembled probe. **b** Photo of the probe during the 3D static magnetic field mapping experiments

## 2.4 The Microwave System

The MW system that drives the probe is based on our homebuilt pulsed ESR microimaging system. It includes a spectrometer, gradient current drivers, and control software. A detailed description of the system is provided elsewhere [28, 31]. In this work, we did not make use of the system's imaging functionality, although in the future some of these capabilities may be useful to improve signal quality (see below).

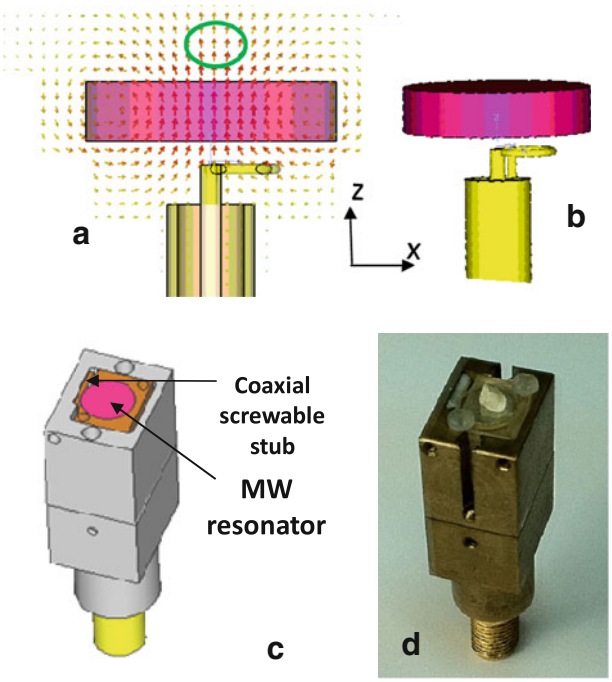


**Fig. 6** MW resonator unit. **a** The calculated MW magnetic field of the resonator and the region of interest from which the signal is picked up (marked with a *green oval*). **b** Perspective view of the resonator, showing the coupling via loop from the bottom. **c** Drawing of the entire resonator assembly with the screwable stub for fine frequency adjustments. **d** Photo of the resonator assembly with a tooth piece placed on it (color figure online)

## 3 Samples

### 3.1 Teeth Samples

The radiation absorbed dose is a measure of the amount of energy deposited in a human body by ionizing radiation. This dose, which is measured in units called "grays" (Gy), equivalent to 1 J per 1 kg of material, is used to predict the outcome of an exposure to radiation. The concentration of paramagnetic defects in the tooth enamel is proportional to the ionized radiation dose; however, this also depends on the specific energy of the radiation [32]. When nuclear events are of concern, the common assumption is to use the energy of a $^{137}$Cs source (662 keV), with the dose defined with respect to water (i.e., a hypothetical person would have $\sim$1 Gy deposited in his oral cavity, rather than the precise J/kg deposited in the enamel). In view of this, the test samples were incisor teeth irradiated according to this standard using a $^{137}$Cs source at the Radiology Department, EPR Center, Dartmouth Medical School. The teeth were placed in full water-equivalent buildup material and positioned at the maximum-dose depth as measured in water. Ideally, we would have liked to use several samples irradiated with doses ranging from 0 to 10 Gy

(which is the relevant range for patient diagnostics, see Sect. 1). In practice, our probe is currently not sensitive enough to tackle with such low doses. Thus, in this work we made use of teeth denoted T10-2 (dose of 15 Gy), T10-4 (30 Gy), and T10-6 (not exposed to irradiation). Additionally, a single molar tooth denoted TR8 was irradiated with a dose of 8 Gy at the Rambam Medical Center Radiation Facility (Haifa, Israel) using an iridium source (340 keV). Two additional teeth, denoted as TNH100 and TNH50, were subjected to gamma irradiation from a $^{60}$Co source ($\sim$1.17 MeV) at the Nahal Sorek Nuclear Research Center (Yavneh, Israel). The amount of radiation deposited in these teeth was determined by comparing their signal to a reference sample of 1-μM deuterated trityl free radical water solution (synthesis described in ref. [33]), using a commercial CW ESR system (X-band EMX model by Bruker). The doses in the TNH100 and the TNH50 teeth were found to be 10,000 and 4,000 Gy, respectively.

### 3.2 Test Samples

Some of the measurements to evaluate the probe's sensitivity were carried out with a sample of 1-mM water solution of deuterated trityl radical and a sample of lithium phthalocyanine (LiPc) solid radical. LiPc crystals are very useful species for ESR measurements because they have a relatively high spin concentration of $10^8$ spins per $(\mu m)^3$ [34], can be stored for long periods of time, and have a minimal effect on a resonator's $Q$ factor. A glass tube (o.d. 0.9 mm) containing LiPc crystals was prepared and sealed under vacuum. The number of spins in this LiPc sample was found to be $\sim 10^{15}$ by comparing it to the signal of the 1-μM trityl reference sample.

## 4 Experimental Results

### 4.1 Evaluation of the Ex Situ Probe's Performance with Calibrated Samples

The performance of the pulsed ESR ex situ biodosimetry probe was evaluated using the LiPc and trityl test samples. The LiPc in the capillary was placed at the center and on top of the ring resonator. The experimental conditions were as follows: frequency of 6.184 GHz, Hahn echo pulse sequence employing two 120° pulses 35-ns long with interpulse separation, $\tau$, of 500 ns and repetition rate of 70 kHz (current software maximum). The total averaging time was 114 s (i.e., 8-M signal acquisitions). The resulting time domain echo signal compared to the noise is plotted in Fig. 7a. The noise in this case was measured with the power amplifier tuned off, and the single-shot SNR for this noise level was $\sim$12.4. A different type of noise measurement was made by adding a field offset of $\sim$30 G using a large external coil. In that case, the transmitted pulse left some ringing, which resulted in an overall noise standard deviation that is larger by a factor of $\sim$2 than the noise measured with the power amplifier off. Figure 7b shows the results of a similar measurement carried out with the trityl sample. Here, the repetition rate was limited to 20 kHz to avoid sample saturation. The total acquisition time was also 114 s and the single-shot SNR was found to be $\sim$1.8.

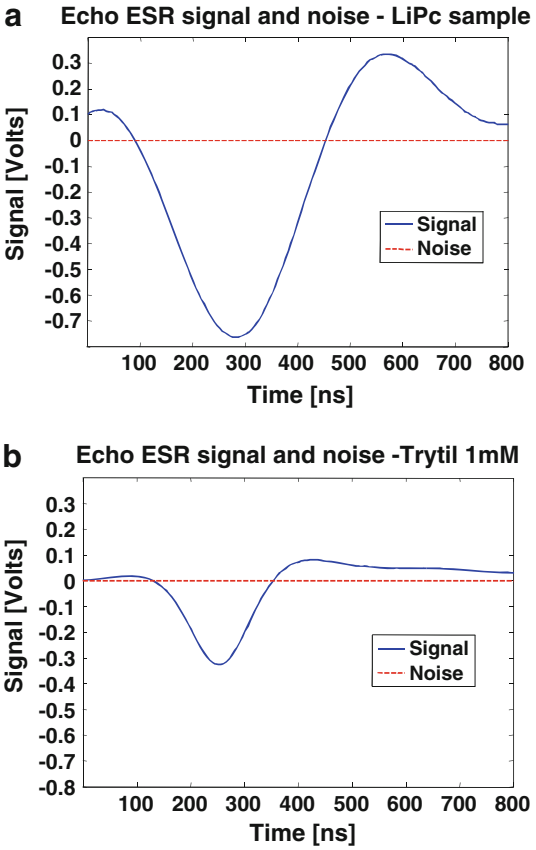


**Fig. 7** **a** ESR signal and noise from the LiPc test sample. The time axis starts at the gate of the acquisition window which starts ~200 ns after the end of the second pulse in the Hahn echo sequence. **b** ESR signal and noise for the 1-mM trityl test sample

## 4.2 Phase Memory Time of Irradiation-Induced Defects in Teeth

The spin–spin relaxation process of paramagnetic defects in the teeth is often explained as an instantaneous diffusion process, and its time dependence following a Hahn echo sequence with interpulse separation delay, $\tau$, is described by a stretched exponential function $S(2\tau) = S(0)e^{\left(-\frac{2\tau}{T_m}\right)^x}$, where $T_m$ is the spin phase memory time [27], and $x$ was found to be ~1 at 130 K and ~0.5 at room temperature [27]. In our present work, the exact behavior of the decay is of no real importance; however, we still wanted to estimate its magnitude as it affects our ability to measure the signal in pulsed-mode ESR. Thus, our analysis assumed a simple exponential decay function for the echo signal ($x = 1$) and fitted the data to this model. We measured $T_m$ to be ~1 μs using our probe with teeth TNH100 and TNH50 while employing a Hahn echo sequence with two identical 120° pulses in which $\tau$ was varied from 500 to 1200 ns in 13 steps.

### 4.3 Spin–Lattice Relaxation Time in Teeth

The spin lattice relaxation time of the paramagnetic defects in the irradiated teeth does not assume a single value and is distributed over a large span of time scales [27]. However, for our current needs, we are only interested in a typical characteristic value in order to determine the maximal repetition rate at which we can efficiently average our data without reaching saturation. Thus, we assume a simple exponential model, in which the ESR signal can be described by $S(T_R) = S(T_R = \infty)\left(1 - e^{\left(-\frac{T_R}{T_1}\right)}\right)$ where $T_R$is the repetition time. The results obtained after performing measurements on teeth TNH100 and TNH50 are $T_1$ of $\sim$5 μs.

### 4.4 CW and Echo-Detected ESR Spectrum of Irradiated Teeth

Here, we provide a comparison of the spectrum of an irradiated tooth (TNH100) as it was measured in CW and field-swept echo-detected pulsed modes. As noted above, prior work found a range of values for $T_m$ [27], which might be attributed to several types of paramagnetic species. The previous work did not provide any spectral information regarding the pulsed results. The present work does not focus on the spectral features and spectral analysis of the irradiated teeth samples, however, it is important to try and find the spectral relation between the signals we are measuring in pulsed mode to the ones detected in CW (which are far-better documented). Figure 8 provides this comparison. An additional measurement was performed in the presence of the LiPc sample in order to facilitate *g*-factor analysis (not shown but used to center the spectrum on the LiPc line). It is apparent that the spectral features in the two measurements are very similar except for a more distorted spectrum at the X-band measurement, probably due to *g* anisotropy that is better resolved at this frequency.

### 4.5 Evaluation of the Performance of the Ex situ Probe used on Teeth

Following these tests, we went ahead and measured the actual incisor teeth irradiated with doses approaching clinically relevant levels (but, as noted in Sect. 3.1—still above the favorable values). The signals were obtained from the teeth denoted above as T10-2, T10-4, T10-6, and TR8. Figure 9 shows the data for teeth T10-4 and T10-2 (T10-6 and TR8 did not give any distinguishable ESR signal). The measurement Hahn echo pulse sequence consisted of two 120° pulses, 35-ns long, with $\tau = 500$ ns. Each sequence was repeated at a repetition rate of 70 kHz for signal averaging (a total of 8 M acquisitions, 114 s). There was difficulty in placing the teeth flat down on the probe's surface (due to the plastic screws that hold the resonator structure); therefore, most of the teeth were positioned with their incisal edge adjacent to the resonator (see Fig. 9c). After the 114-s collection times, the SNR for the T10-4 and T10-2 teeth was $\sim$33 and $\sim$27, respectively, which translates into a single-shot SNR of $\sim$0.012 and 0.01. The resonance frequency

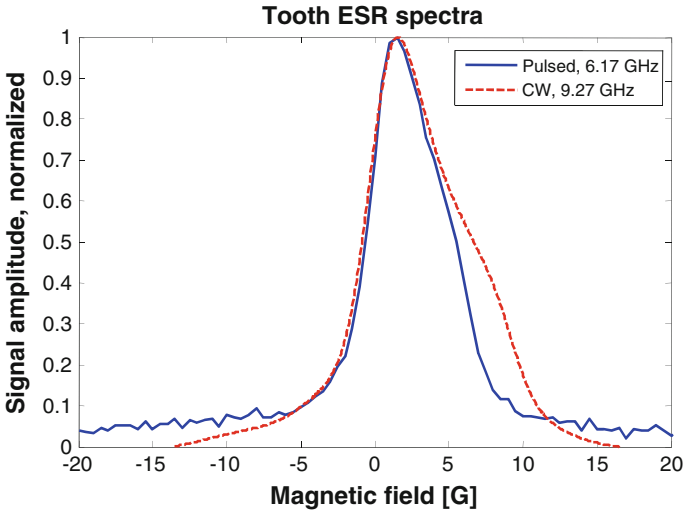


**Fig. 8** CW and echo-detected pulsed spectra for irradiated tooth. The CW experiments were carried out on a Bruker EMX system at 9.27 GHz with 1-Gauss modulation amplitude. The field-swept echo-detected experiments were carried out with our 6.18-GHz resonator, placed in a regular homogenous electromagnet. This measurement employed a Hahn echo sequence with interpulse delay $\tau = 700$ ns and pulse lengths of 100 ns

shift induced by the teeth was typically $-10$ MHz, with a slight reduction in $Q$ from $Q_u = 500$ in the empty resonator to $Q_u = 400$.

## 5 Discussion

The measured properties of the static field source and the microwave resonator closely follow the results obtained by the detailed finite element designs. The results in Figs. 7 and 9 clearly demonstrate the functionality of the newly developed ex situ ESR probe. However, the main issue that needs to be discussed in detail is the probe's spin sensitivity and its corresponding capability to accurately qualify the radiation absorbed dose in teeth. This sensitivity analysis will be provided below with reference to the predicted theoretical sensitivity.

The number of spins detectable with an SNR of 1 in a single-shot data acquisition is provided by [35]:

$$\text{Sensitivity}^{\text{spins}}_{\text{single shot}} \approx \frac{8\sqrt{V_c}\sqrt{k_b T(1/\pi T_2^*)}}{\mu_B \omega_0 \sqrt{2\mu_0}} \sqrt{\frac{\omega_0}{Q_u}} B_F. \quad (1)$$

The symbol $V_c$ represents the resonator's effective volume [28, 29, 35, 36], which is equal to the volume of a small hypothetical sample $V_v$ (for example, $(1\ \mu\text{m})^3$) usually located at the point where the resonator's microwave magnetic field is maximal, divided by the filling factor [37] of this small sample [36]. $k_b$ is the Boltzmann constant, $T$ is the temperature, $\omega_0$ is the electron's Larmor angular

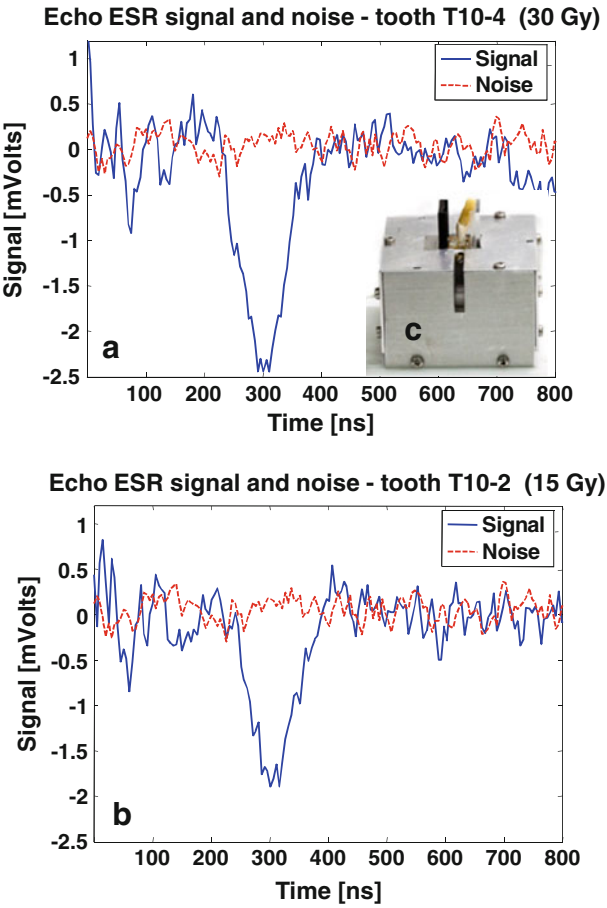


**Fig. 9** ESR signal and noise for the T10-4 (**a**) and T10-2 (**b**) irradiated teeth. *Inset* (**c**) shows a photo of the teeth placed on its incisal edge during measurement

frequency, $\mu_0$ is the free-space permeability, and $Q_u$ is the unloaded quality factor of the resonator. Here, we assumed that the bandwidth of excitation is chosen to match the linewidth of the imaged paramagnetic species in the sample, $\Delta f = 1/\pi T_2^*$. $B_F$ is the Boltzmann population factor $B_F = \frac{1+e^{-\frac{\hbar\omega_0}{k_B T}}}{1-e^{-\frac{\hbar\omega_0}{k_B T}}}$, and $\mu_B$is Bohr's magneton.

Plugging the relevant parameters for the LiPc experiment into Eq. (1) (i.e., $T_2^* = 200$ ns—see Fig. 7a, $B_F = 0.2125$ T, $V_c = 3.5 \times 10^{-8}$ m$^3$, $Q_u = 500$, $\omega_0 = 3.88 \times 10^{10}$ rad/s) provides us with a theoretical single-shot spin sensitivity of $\sim 4 \times 10^{12}$ spins for a point sample located just above the resonator. This means that our $10^{15}$-spin LiPc sample should have given a single-shot SNR of $\sim 10^{15}/4 \times 10^{12} = 250$. This theoretical value is better than our actual result by a factor of $\sim 20$, which may be due to a variety of factors such as $T_2$ relaxation, sample calibration errors, non-ideal pulse sequence excitation, or other unknown experimental errors.

For the 1-mM trityl solution, the effective excited volume of a sample is approximately 1 μL, which means that we measured $\sim 6 \times 10^{14}$ spins. This leads to an expected single-shot spin sensitivity of $\sim 7.3 \times 10^{12}$ spins ($Q_u = 200$ due to the dielectric losses of the solution and $T_2^* = 150$ ns). Thus, the theoretical single-shot SNR for a point sample with these properties, just above the resonator, is $\sim 82$. If we compare this to our measured sensitivity, we still lack a factor of $\sim 45$. The reason for that, in addition to the ones mentioned above in the LiPc case, may be the spreading of this sample over a relatively large volume above the resonator where its sensitivity greatly degrades.

The expected single-shot spin sensitivity for the teeth sample can again be calculated from Eq. (1), but here $T_2^* = 100$ ns and $Q_u = 400$, which results in a value of $\sim 2.5 \times 10^{12}$ spins. Based on the expected specific spin number of $2.8 \times 10^{13}$ spins $Gy^{-1}$ $g^{-1}$ [9], 1 μL of teeth irradiated with 15 Gy should have $\sim 1.2 \times 10^{12}$ spins (given enamel density of $\sim 2.8$ [38]). This means that ideally we should have obtained a single-shot SNR of $\sim 0.5$ for the T10-2 tooth, while in practice we obtained only $\sim 0.01$. Again, we see some discrepancy that is similar to what we found for the "point-like" LiPc and the volumetric trityl sample, probably due to similar reasons, to which the possibility of attachment issues (as can be seen in Fig. 9c) may be added. Such attachment issues can also explain why the T10-4 tooth's signal is not a factor of two larger than the T10-2's signal.

The sensitivity that we obtained with the current probe in our experiments is not sufficient for immediate clinical applications. The results provided in Fig. 9 show that for a dose of 15 Gy the SNR is ~4–5, meaning that a dose of less than 4 Gy would probably be very hard to measure with the current setup. Better future design of the probe, as described in the conclusion section below, can bring its sensitivity to the required 0.5–0.25 Gy level. In addition to sensitivity improvement, the future probe must also show good linear response in all radiation doses from ~0.5–10 Gy and should have high repeatability. However, these characteristics can be measured only once sufficient sensitivity is obtained.

## 6 Conclusions and Future Outlook

A new type of self-contained ex situ ESR probe operating in pulsed mode for tooth-based biodosimetry has been presented. The measured properties of the probe in terms of static and MW fields closely follow the design, while its sensitivity is lower than excepted. The new approach presented here addresses many of the above-mentioned problems typical of conventional in vivo CW-based low-field ESR systems:

(1) The magnet is small (with typical dimensions of a few centimeters), due to the tiny volume of interest required just above its surface. Furthermore, the system can be used with a static field that has a *fixed gradient* rather than high *homogeneity* (since the use of a pulsed ESR echo sequence focuses the signal). This also helps to decrease the size of the magnet and makes its design and construction relatively simple and more tolerant to variations. (2) The spot where the magnetic field is optimal aligns automatically with the resonator, because they are mechanically fixed

together and brought forward toward the tooth. (3) The system can measure a small, *well-defined volume* just below the tooth surface and could in principle also provide a 1D slice across the tooth. This can allow a good assessment of the spin *concentration* directly from the ESR signal, since the small detected volume contains only bulk tooth enamel. Furthermore, the possibility of obtaining signals selectively from a volume *within* the tooth eliminates the contribution of surface defects. (4) The new probe can provide a solution for obtaining a viable signal in measurements made in children's and toddler's teeth. (5) The probe is not inserted into the mouth but rather brought to the incisor tooth (see Fig. 1), thereby minimizing the need for disposable sterile components. (6) The system is designed for pulsed operation, where resonator stability and mechanical movements are a much lesser concern. The use of tiny dielectric resonators eliminates the need for high-power amplifiers and all measurements can be done with low-power cheap solid-state sources. (7) Although we probe a volume that is $\sim$500 times smaller than in most current low-frequency systems ($\sim$1 μL vs. $\sim$0.5 mL), radiation dose sensitivity should in principle be comparable and even better. This is because spin sensitivity increases as $B_0^2$ increases (assuming there are no depth penetration problems, which is not an issue for teeth), and the filling factor for the small volume we measure increases as resonator size decreases. This means that moving from the L-band to the C-band (and in the next iteration, possibly to the X/Ku-band) improves spin sensitivity by two or more orders of magnitude. Also, in the L-band the wire-based resonators have a rather low $Q$ compared to the small dielectric resonator employed here, which increases sensitivity by a factor of $\sim$2. (8) *Field deployment* The probe itself weighs $\sim$1 kg, while the other parts of the system can be kept to minimum size and weight.

As briefly mentioned above, future iteration of the probe can make use of even higher static fields with a better resonator/static field alignment. The probe should have a more concave geometry (for both magnet and resonator) facilitating a better ergonomic alignment of the front of the face/tooth with the probe. Another issue of concern that can be dealt with in the future is minimizing the ring down signals. This can be achieved by adding a small bias coil to the probe itself. This coil unit will produce a small static field that could be switched on/off quickly to reduce the ringing. This can be achieved by driving the coil through a fast current driver (similar to the one used in our ESR microimaging experiments [31]). In such a fast phase-cycling scheme, the small field bias is turned off/on for subtraction between the on/off resonance signal at a fast repetition rate of $\sim$200 kHz. Under such conditions, the residual ringing would be greatly attenuated, thereby making it possible to reduce the interference to the signal and also $\tau$, and thus increase the signal (minimizing the $T_m$ effect). The small coil can also be used to produce a small static-field bias, in case the resonance frequency of the resonator changes. The cumulative effects of all these improvement can increase significantly the spin (and radiation dose) sensitivity of the probe and thus reach a point where it can become a clinically significant and a useful tool in the future.

**Acknowledgments** This work was partially supported by a pilot project from NIH/NIAID through Dartmouth College and by Grant #201665 from the European Research Council (ERC). We thank

Dr. Ben Williams from Dartmouth College and Dr. Raquel Bar-Deroma from Rambam Hospital and their teams for supplying us with irradiated teeth.

## References


1. S.K. Misra (ed.), *Multifrequency Electron Paramagnetic Resonance, Theory and Applications* (Wiley-VCH, Berlin, 2011)
2. P. Fattibene, F. Callens, Appl. Radiat. Isot. **68**, 2033–2116 (2010)
3. M. Ikeya, M.R. Zimmerman, N. Whitehead, *New Applications of Electron Spin Resonance: Dating, Dosimetry and Microscopy* (World Scientific, Singapore, 1993)
4. S. Vatnitsky, *Use of Electron Paramagnetic Resonance Dosimetry with Tooth Enamel for Retrospective Dose Assessment*. (International Atomic Energy Agency, 2002). http://www-pub.iaea.org/MTCD/publications/PDF/te_1331_web.pdf
5. R.C. Wilkins, H. Romm, T.C. Kao, A.A. Awa, M.A. Yoshida, G.K. Livingston, M.S. Jenkins, U. Oestreicher, T.C. Pellmar, P.G.S. Prasanna, Radiat. Res. **169**, 551–560 (2008)
6. H.M. Swartz, G. Burke, M. Coey, E. Demidenko, R. Dong, O. Grinberg, J. Hilton, A. Iwasaki, P. Lesniewski, M. Kmiec, K.M. Lo, R.J. Nicolalde, A. Ruuge, Y. Sakata, A. Sucheta, T. Walczak, B.B. Williams, C.A. Mitchell, A. Romanyukha, D.A. Schauer, Radiat. Meas. **42**, 1075–1084 (2007)
7. B.B. Williams, R.H. Dong, M. Kmiec, G. Burke, E. Demidenko, D. Gladstone, R.J. Nicolalde, A. Sucheta, P. Lesniewski, H.M. Swartz, Health Phys. **98**, 327–338 (2010)
8. B.B. Williams, R.H. Dong, A.B. Flood, O. Grinberg, M. Kmiec, P.N. Lesniewski, T.P. Matthews, R.J. Nicolalde, T. Raynolds, I.K. Salikhov, H.M. Swartz, Radiat. Meas. **46**, 772–777 (2011)
9. G.M. Hassan, E. Aboelezz, A. El-Khodary, H.M. Eissa, Nucl. Instrum. Meth. B **268**, 2329–2336 (2010)
10. J.M. Wiener, J. Tilly, Int. J. Epidemiol. **31**(4), 776–781 (2002)
11. H.M. Swartz, A.B. Flood, B.B. Williams, R.H. Dong, S.G. Swarts, X.M. He, O. Grinberg, J. Sidabras, E. Demidenko, J. Gui, D.J. Gladstone, L.A. Jarvis, M.M. Kmiec, K. Kobayashi, P.N. Lesniewski, S.D.P. Marsh, T.P. Matthews, R.J. Nicolalde, P.M. Pennington, T. Raynolds, I. Salikhov, D.E. Wilcox, B.I. Zaki, Health Phys. **103**, 255–267 (2012)
12. J.A. Jackson, L.J. Burnett, J.F. Harmon, J. Mag. Res. **41**, 411–421 (1980)
13. G. Eidmann, R. Savelsberg, P. Blumler, B. Blumich, J. Magn. Reson., Ser. A **122**, 104–109 (1996)
14. P.J. McDonald, B. Newling, Rep. Prog. Phys. **61**, 1441–1493 (1998)
15. M.D. Hurlimann, D.D. Griffin, J. Magn. Reson. **143**, 120–135 (2000)
16. R.J.S. Brown, R. Chandler, J.A. Jackson, R.L. Kleinberg, M.N. Miller, Z. Paltiel, M.G. Prammer, Concept Magn. Res. **13**, 335–413 (2001)
17. B. Blumich, J. Perlo, F. Casanova, Prog. Nucl. Magn. Reson. Spectrosc. **52**, 197–269 (2008)
18. G. Goelman, M.G. Prammer, J. Magn. Reson., Ser. A **113**, 11–18 (1995)
19. R. Haken, B. Blumich, J. Magn. Reson. **144**, 195–199 (2000)
20. A. Scharfenecker, I. Ardelean, R. Kimmich, J. Magn. Reson. **148**, 363–366 (2001)
21. J. Perlo, F. Casanova, B. Blumich, J. Magn. Reson. **166**, 228–235 (2004)
22. A. Blank, G. Alexandrowicz, L. Muchnik, G. Tidhar, J. Schneiderman, R. Virmani, E. Golan, Magn. Reson. Med. **54**, 105–112 (2005)
23. J. Schneiderman, R. Wilensky, A. Weiss, E. Samouha, L. Muchnik, M. Chen-Zion, M. Ilovitch, E. Golan, A. Blank, M. Flugelman, Y. Rozenman, R. Virmani, J. Am. Coll. Cardiol. **45**, 1961–1969 (2005)
24. A. Blank, S. Ish-Shalom, L. Shtirberg, Y. Zur, Magn. Reson. Med. **62**, 1585–1596 (2009)
25. P.J. McDonald, A. Akhmerov, L.J. Backhouse, S. Pitts, J. Pharm. Sci. **94**, 1850–1860 (2005)
26. B. Blumich, V. Anferov, S. Anferova, M. Klein, R. Fechete, M. Adams, F. Casanova, Concept Magn. Res. **15**, 255–261 (2002)
27. H. Sato, B.A. Filas, S.S. Eaton, G.R. Eaton, A.A. Romanyukha, R. Hayes, A.M. Rossi, Radiat. Meas. **42**, 997–1004 (2007)
28. A. Blank, E. Suhovoy, R. Halevy, L. Shtirberg, W. Harneit, Phys. Chem. Chem. Phys. **11**, 6689–6699 (2009)
29. A. Blank, J.H. Freed, Isr. J. Chem. **46**, 423–438 (2006)
30. A. Blank, in *Multifrequency Electron Paramagnetic Resonance*, ed. by S. Misra, Chap. 19 (Wiley-VCH, Berlin, 2011)
31. L. Shtirberg, Y. Twig, E. Dikarov, R. Halevy, M. Levit, A. Blank, Rev. Sci. Instrum. **82**, 043708 (2011)

32. V.A. Kirillov, I.I. Kuchuro, J. Appl. Spectrosc. **77**, 132–139 (2010)
33. Y. Talmon, L. Shtirberg, W. Harneit, O.Y. Rogozhnikova, V. Tormyshev, A. Blank, Phys. Chem. Chem. Phys. **12**, 5998–6007 (2010)
34. K.J. Liu, P. Gast, M. Moussavi, S.W. Norby, N. Vahidi, T. Walczak, M. Wu, H.M. Swartz, Proc. Natl. Acad. Sci. USA **90**, 5438–5442 (1993)
35. Y. Twig, E. Suhovoy, A. Blank, Rev. Sci. Instrum. **81**, 104703 (2010)
36. A. Blank, C.R. Dunnam, P.P. Borbat, J.H. Freed, J. Magn. Reson. **165**, 116–127 (2003)
37. C.P. Poole, *Electron Spin Resonance : A Comprehensive Treatise on Experimental Techniques* (Wiley, New York, 1983)
38. J.A. Weatherell, Br. Med. Bull. **31**, 115–119 (1975)